Графен и топологические изоляторы

Откуда берется линейный спектр ?

1. Релятивистский спектр массивных частиц:

   $E = c[(mc)^2 + p^2]^{1/2} \rightarrow mc^2 + p^2/2m$

2. Нейтрино

   $E = c\,\mathbf{p\sigma} = cp\,\mathbf{n\sigma}$ $\qquad$ $\mathbf{n\sigma} = (+-)\,1/2$

   спиральные состояния

   вектор $\boldsymbol{\sigma}$ необходим для линейного спектра

3. «Обычные» массивные электроны в нерелятивистском пределе имеют спин, но он не связан с орбитальным движением

р е л я т и в и с т с к и м с п е к т р о м к а к э л е м е н т а р н ы е в о з б у ж д е н и я в к х

1. Графен

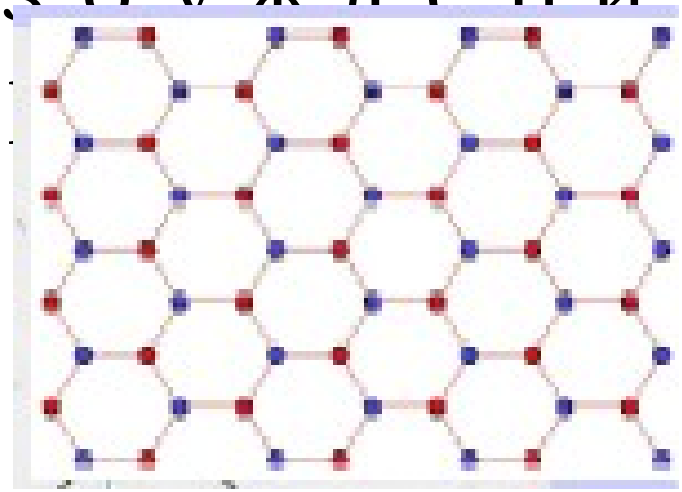

о п о л о г и ч е с к и е и з о л я т о р ы

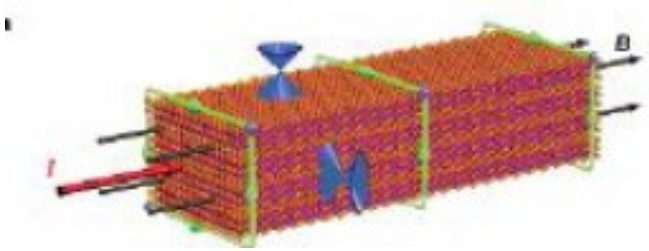

Interesting Physical Properties

Semimetal (zero bandgap): electrons and holes coexist

Massless Dirac electrons, d=2

Graphene electron band structure,
mimic Dirac electrons at points K and K'

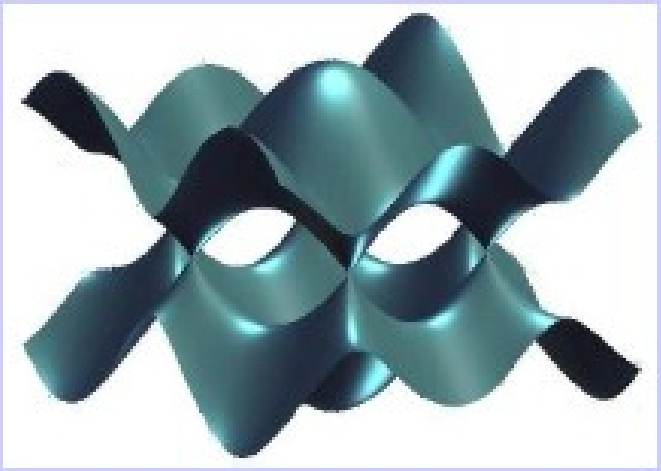

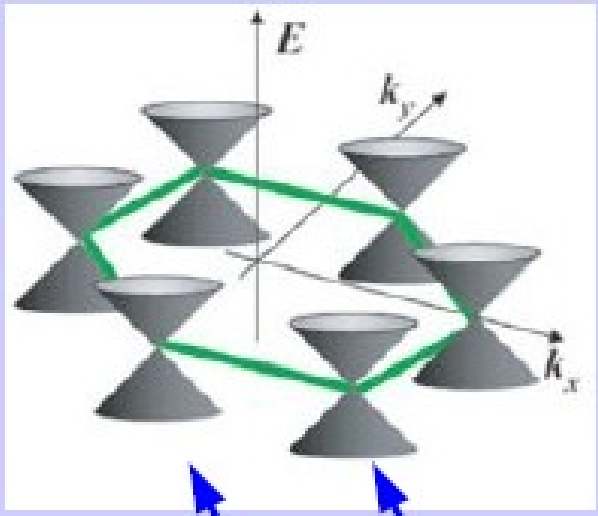

Manifestations: “relativistic” Lorentz invariance
with Fermi velocity instead of light speed

"Half-integer" Quantum Hall Effect

Single-layer graphene:
QHE plateaus observed at

$$\nu = 4 \times (0, \pm 1/2, \pm 3/2 \ldots)$$

=2x2 spin and valley degeneracy

Manifestation of relativistic Dirac electron properties

Landau level spectrum with very high cyclotron energy (1000K)

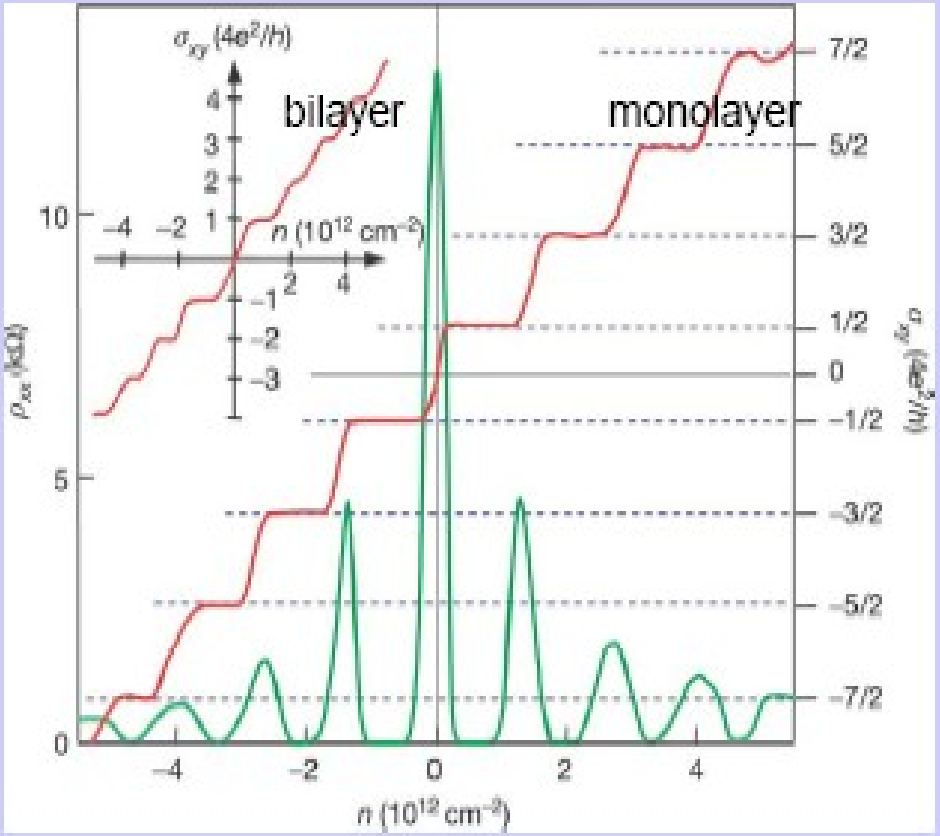

Novoselov et al, 2005, Zhang et al, 2005

Recently: QHE at T=300K

Recently: Graphene devices

Devices in patterned graphene:
quantum dots (Manchester),
nanoribbons (IBM, Columbia);

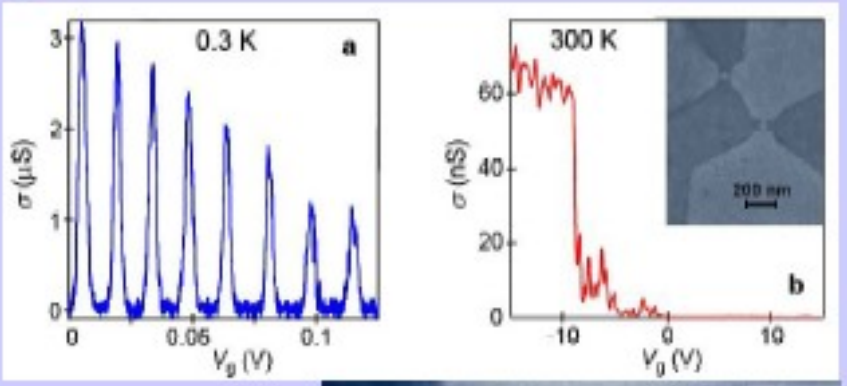

Local density control (gating):
p-n and p-n-p junctions

(Stanford, Harvard, Columbia)

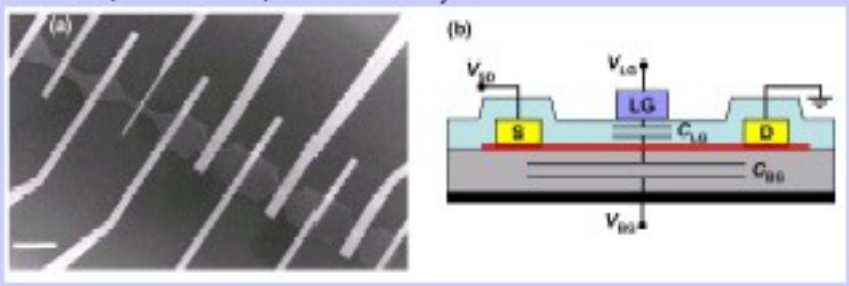

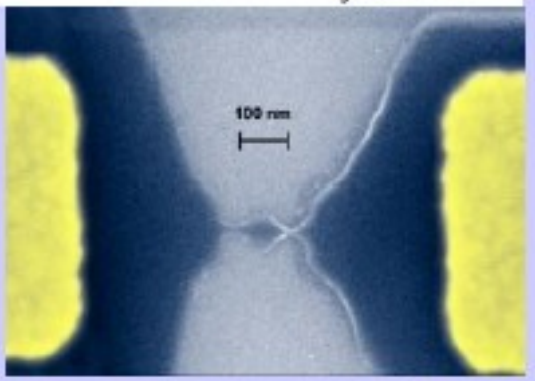

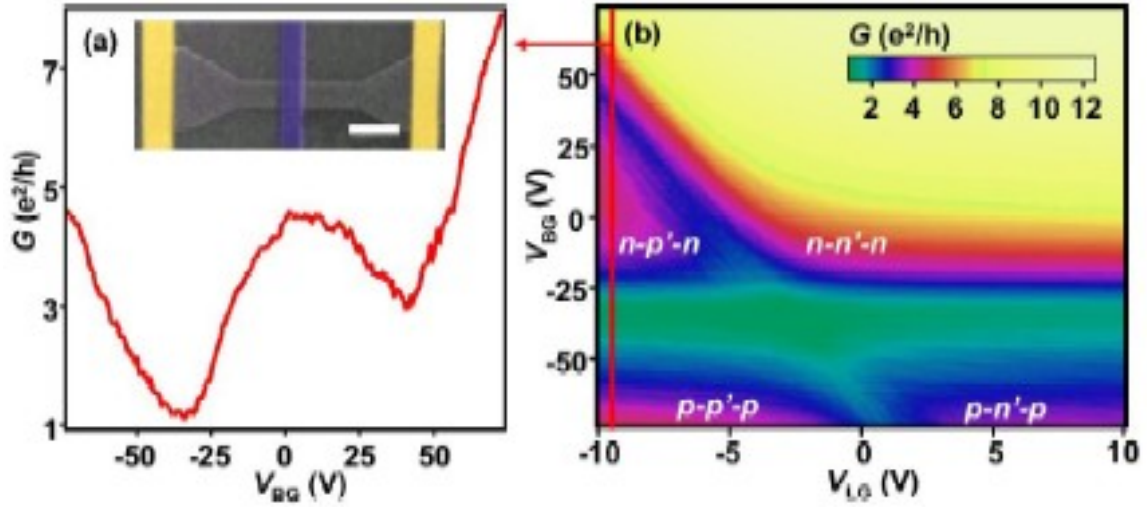

Equal or opposite polarities of charge carriers in the same system (electrons and holes coexist)

Electron properties of graphene

GRAPHENE ALLOTROPES

3D 2D 1D 0D

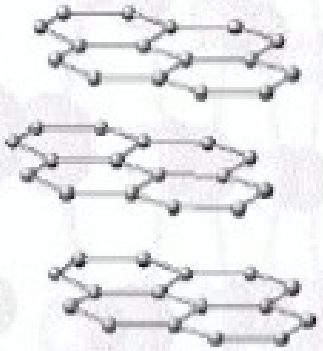

Graphite

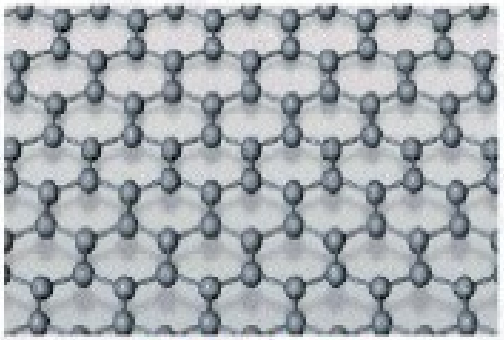

graphene

PRESUMED
NOT TO EXIST
IN THE FREE STATE

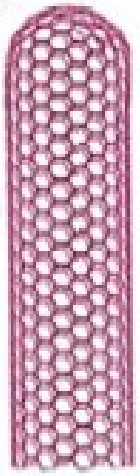

Carbon Nanotube

multi-wall:
1952 to *Iijima 1991*
single-wall: 1993

Buckyballs

Kroto et al 1985

Tight-binding model on a honeycomb lattice

Conduction band

Valence band

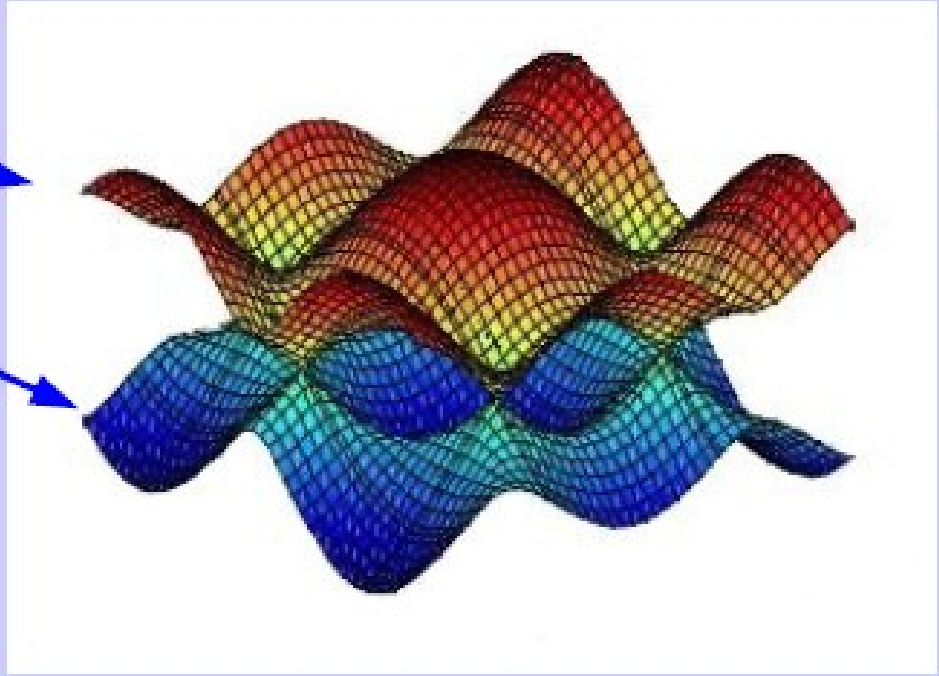

Dirac model:

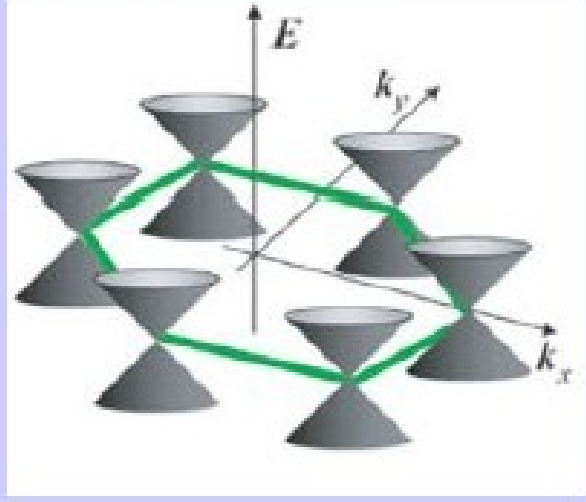

K K'

Velocity v = dE/dp=10^8 cm/s = c/300

Density of states linear in E,
and symmetric N(E)=N(-E)

Other effects: next-nearest neighbor hopping; spin-orbital coupling; trigonal warping (ALL SMALL)

Real space, reciprocal space

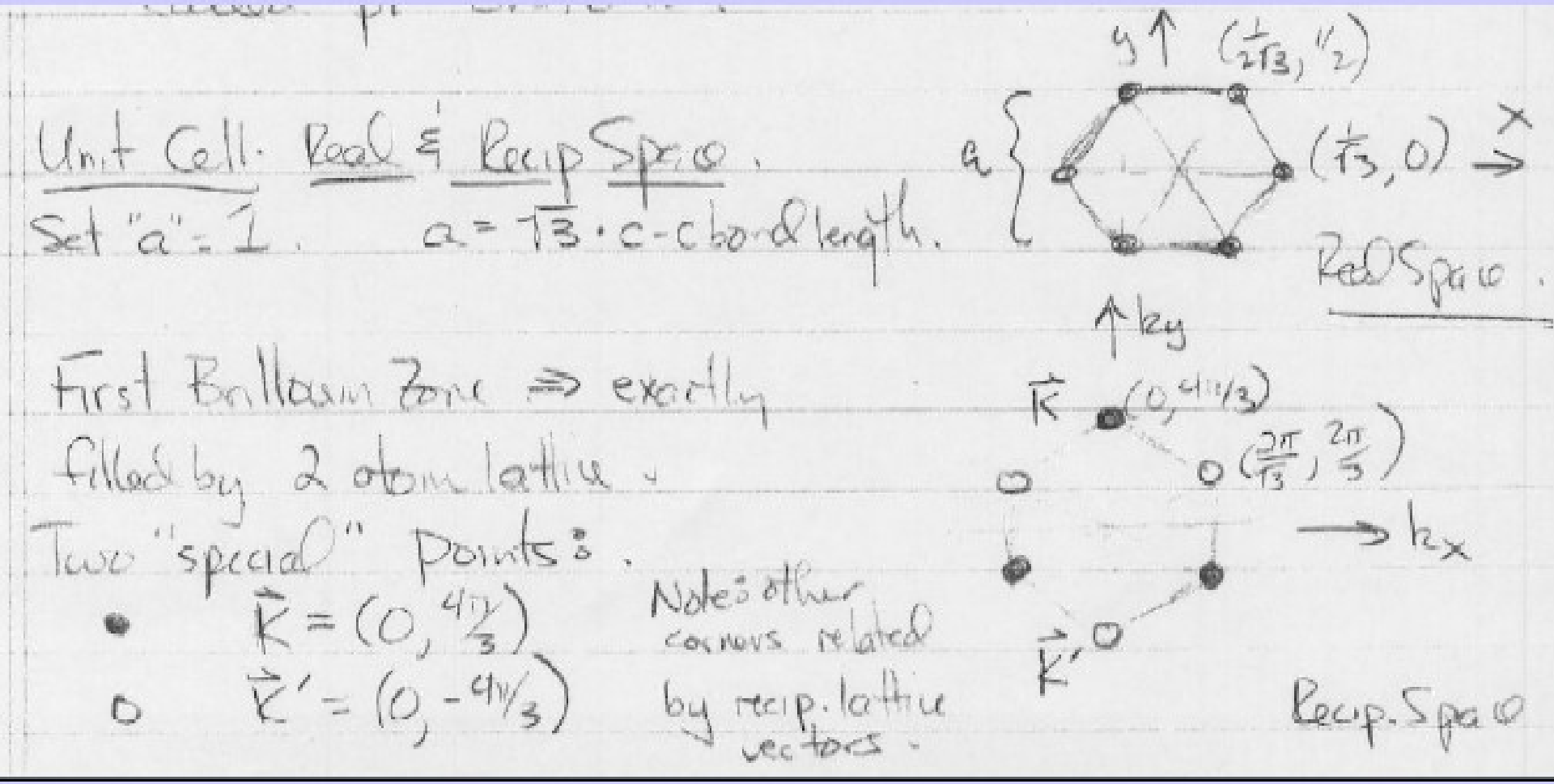

Graphene: tight-binding model

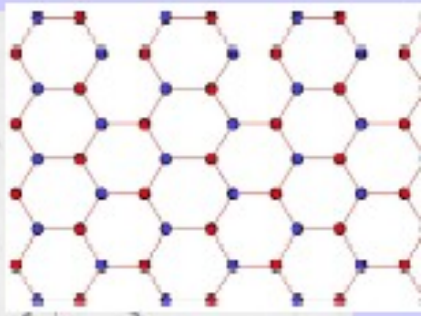

Tight Binding Model:

Assume N-N hopping with element t.

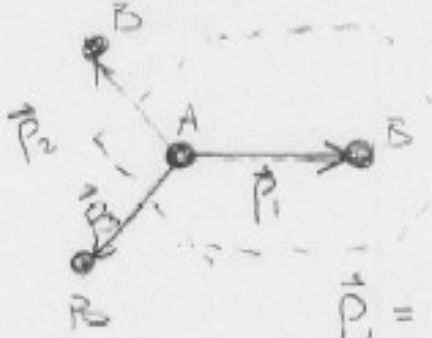

$\vec{\rho}_1 = (\frac{\pm}{\sqrt{3}}, 0)$

$\vec{\rho}_{2,3} = (-\frac{\pm}{2\sqrt{3}}, \pm\frac{1}{2})$

Need two #'s to describe basis

Write as column vector.

$\begin{pmatrix} 1 \\ 0 \end{pmatrix}$ ⇒ electron on A $\quad \begin{pmatrix} 0 \\ 1 \end{pmatrix}$ ⇒ electron on B.

⇒ Hopping is off-diagonal (from A to B)

Assume $\psi(r) = \psi(0)\, e^{i\vec{k}\cdot\vec{r}}$ Bloch waves.

Then:

$$\mathcal{H} = \begin{pmatrix} 0 & \overbrace{t\sum_i e^{-i\vec{k}\cdot\vec{\rho}_i}}^{h^*} \\ \underbrace{t\sum_i e^{i\vec{k}\cdot\vec{\rho}_i}}_{h} & 0 \end{pmatrix} \Rightarrow E = \pm|t|^2 \left|\sum e^{i\vec{k}\cdot\vec{\rho}_i}\right|^2 = \pm|h|$$

↑ Two roots correspond to π & π^* bands.

Electronic Properties of Graphene

Graphene

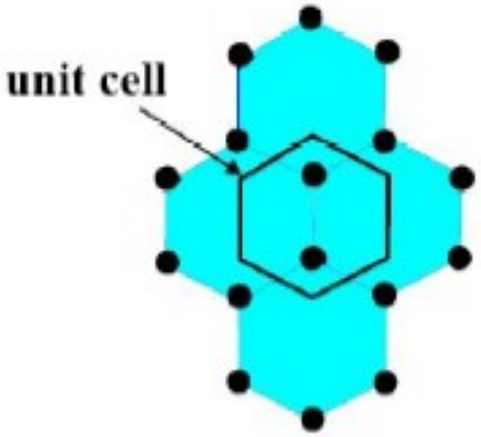

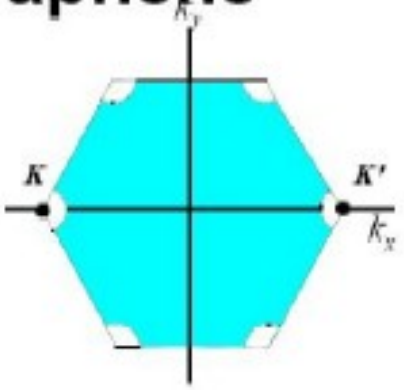

First Brillouin Zone

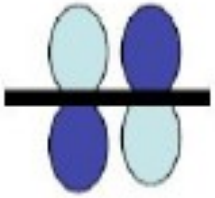

Anti-Bonding Orbitals

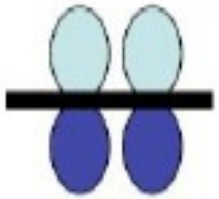

Bonding Orbitals

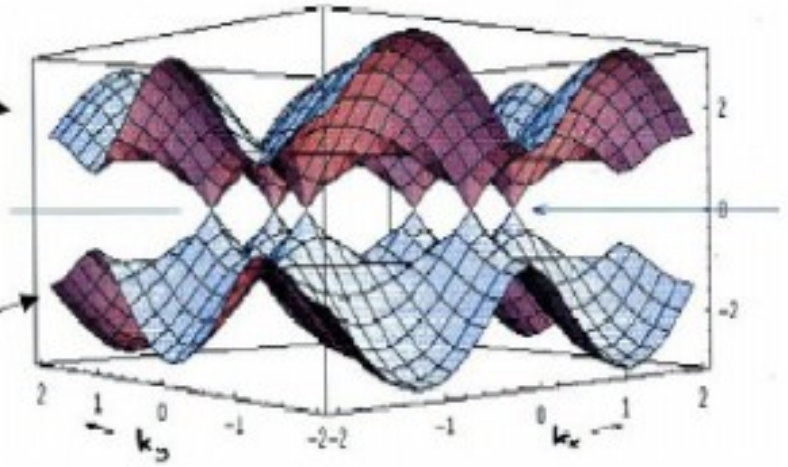

Linearize H near K and K'

$\Rightarrow$ see graph.

$$h = t\left[e^{ik_x/\sqrt{3}} + e^{-\frac{ik_x}{2\sqrt{3}}} 2\cos(k_y/2)\right]$$

Interesting case: $\vec{K} = \vec{K}' = (0, 4\pi/3)$.

$$h = t\left[1 + 2\cos(2\pi/3)\right] = t\left[1 + 2(-1/2)\right] = 0.$$

$E(\vec{k}) = \pm 0$ $\leftarrow$ same energy

$\Rightarrow$ **Gap Vanishes at $\vec{K}$ & $\vec{K}'$**

What about nearby $\vec{k}$ point?

$$\vec{k} = \vec{K} + \delta\vec{k} \Rightarrow k_x = \delta k_x \quad k_y = \frac{4\pi}{3} + \delta k_y \quad (\delta k \ll 1)$$

$$h = t\left[\left(1 + i\delta k_x/\sqrt{3}\right) + \left(1 - i\delta k_x/2\sqrt{3}\right) 2\left[-\frac{1}{2} + \left(-\sin\left(\frac{2\pi}{3}\right)\right)\delta k_y/2\right]\right]$$

$$= t\left[\frac{\sqrt{3}}{2} i\delta k_x - \frac{\sqrt{3}}{2}\delta k_y\right.$$

$$= \frac{\sqrt{3}}{2} t\left(i\delta k_x - \delta k_y\right). \quad \text{or:}$$

$$\mathcal{H} = -\frac{\sqrt{3}}{2} t \begin{pmatrix} 0 & i\delta k_x + \delta k_y \\ -i\delta k_x + \delta k_y & 0 \end{pmatrix} = A\,\vec{\sigma}\cdot\vec{p}$$

2D Massless Dirac Hamilt.

Low energy properties I

Band Structure – low energies.

Massless Dirac Fermions.

Sublattice structure $\Longleftrightarrow$ "spin" → $\pm\frac{1}{2}(1,1)$ → bonding → $+S_x$

$\pm\frac{1}{2}(1,-1)$ → antibonding → $-S_x$ ..

"spin" points along propagation direction (wait prove).

Putting in units, etc.:

$$E_\pm(\delta\vec{k}) = \pm \hbar v_F (\delta k_x^2 + \delta k_y^2)^{1/2}$$

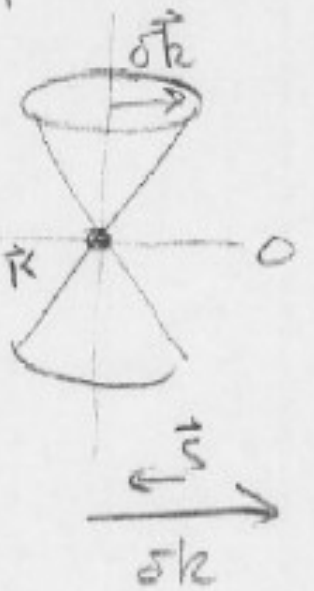

At K', same except "spin" is antiparallel to $\delta\vec{k}$.

$\Rightarrow$ left $\neq$ right handed fermions

$\Rightarrow$ Very Unusual 2D system!

$\Rightarrow$ Zero Bandgap Semiconductor.

left -handed

Low energy theory:
2D massless
Dirac Fermions

Dirac (*k*•*p*) Hamiltonian

$$H = \hbar v_F \sigma \cdot k$$

right-handed

$$E = b\hbar v_F |k|$$

$$|k\rangle = \frac{1}{\sqrt{2}} e^{ik\cdot r} \begin{pmatrix} -ibe^{-i\theta_k/2} \\ e^{i\theta_k/2} \end{pmatrix}$$

"spin" = molec. orbital state

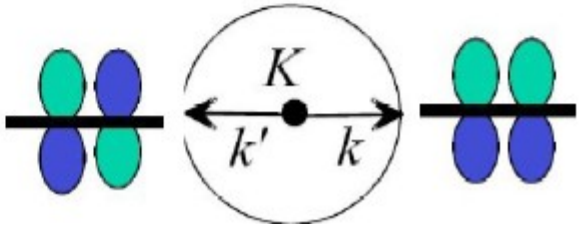

1: Пусть есть двухслойный графен. Какой там сп
изких энергиях?

Relativistic electron in magnetic field

$$E_n = \mathrm{sgn}(n)|n|^{1/2}\epsilon_0, \quad \epsilon_0 = \hbar v_0 \left(2eB/\hbar c\right)^{1/2}$$

Particle-hole symmetric; has a *zero mode*

$E_n \propto \sqrt{n}, \sqrt{B}$

Separation between low-lying LL is very large, $1000\,\mathrm{K}$ at $B = 10\,\mathrm{T} \longrightarrow$ *room temperature QHE*

Explanation: $H_{\text{Pauli-Schroedinger}} = 2m(H_{\text{Dirac}})^2$

ча 2 Найти весь спектр графена в магнитном по

Klein tunneling

Klein paradox: transmission of relativistic particles is unimpeded even by highest barriers
Reason: negative energy states;
Physical picture: particle/hole pairs

Katsnelson, Novoselov, Geim

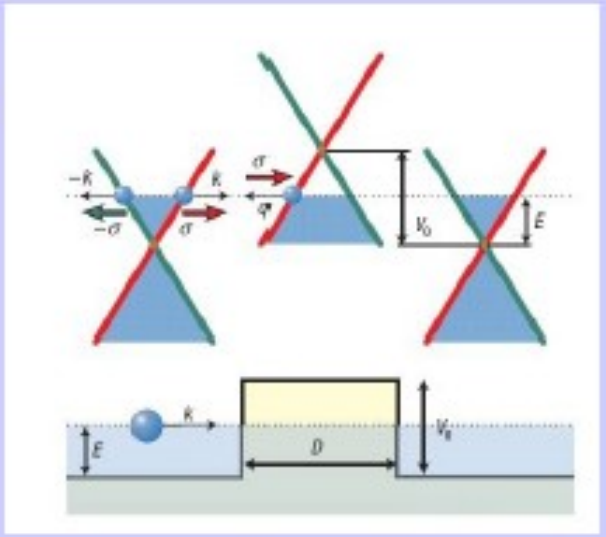

Example: potential step

$$V(x) = \begin{cases} V_0, & 0 < x < D, \\ 0 & \text{otherwise.} \end{cases}$$

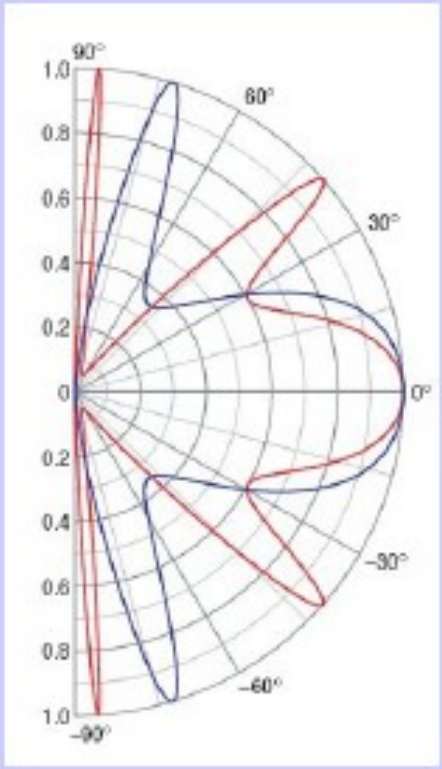

Transmission angular dependence

$$\psi_1(x,y) = \begin{cases} (e^{ik_x x} + re^{-ik_x x})e^{ik_y y}, & x < 0, \\ (ae^{iq_x x} + be^{-iq_x x})e^{ik_y y}, & 0 < x < D, \\ te^{ik_x x + ik_y y}, & x > D, \end{cases}$$

$$\psi_2(x,y) = \begin{cases} s(e^{ik_x x + i\phi} - re^{-ik_x x - i\phi})e^{ik_y y}, & x < 0, \\ s'(ae^{iq_x x + i\theta} - be^{-iq_x x - i\theta})e^{ik_y y}, & 0 < x < D, \\ ste^{ik_x x + ik_y y + i\phi}, & x > D, \end{cases}$$

Chiral dynamics of massless Dirac particles: no backward scattering (perfect transmission at zero angle)

Limit of extremely high barrier: finite T

$$T = \frac{\cos^2\phi}{1 - \cos^2(q_x D)\sin^2\phi}.$$

Задача 3: Вычислить коэффициент прохождения

Топологические изоляторы

- Простейший пример: зонный диэлектрик (3-мерный или 2-мерный), образующий устойчивые поверхностные проводящие состояния
- Обобщение: любая система с щелью в

Предистория:

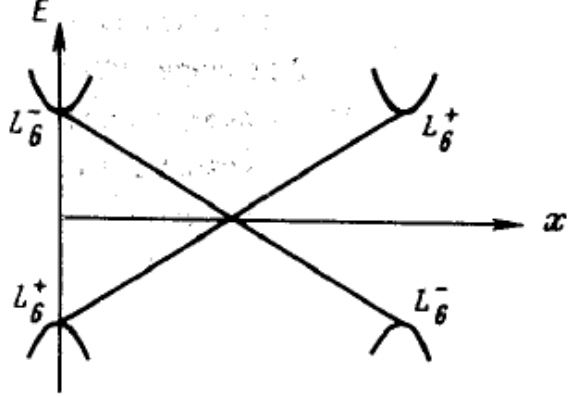

Рис. 1. Инверсия зон $L_6^{\pm}$ в $Pb_{1-x}Sn_xTe(Se)$

Письма в ЖЭТФ, том 42, вып. 4, стр. 145 – 148 *25 августа 1985 г.*

БЕЗМАССОВЫЕ ДВУМЕРНЫЕ ЭЛЕКТРОНЫ В ИНВЕРСНОМ КОНТАКТЕ

Б.А.Волков, О.А.Панкратов

Предложен новый тип полупроводниковых структур на основе контакта двух материалов с взаимно инвертированными зонами. Качественной особенностью такого контакта является наличие в нем независящих от вида переходной области электронных состояний с линейным двумерным спектром. Определены свойства инверсного контакта во внешнем магнитном поле.

В двухзонном приближении энергетический спектр такого контакта описывается уравнением Дирака с зависящей от координаты z шириной запрещенной зоны:

$$\begin{pmatrix} -\epsilon & i\epsilon_g/2 + \vec{\sigma}\mathbf{p} \\ -i\epsilon_g/2 + \vec{\sigma}\mathbf{p} & -\epsilon \end{pmatrix} \begin{pmatrix} \chi_- \\ \chi_+ \end{pmatrix} = 0, \qquad (1)$$

где $\vec{\sigma}$ – матрицы Паули, $\mathbf{p} = -i\hbar(v_\perp \nabla_x, v_\perp \nabla_y, v_\parallel \nabla_z)$, ось z направлена по тригональной оси кристалла, $\chi_\pm$ – двухкомпонентные спиноры. Если по разные стороны контакта знаки ϵ_g различны ($\epsilon_g(-\infty) < 0, \epsilon_g(+\infty) > 0$), то независимо от конкретного вида функции $\epsilon_g(z)$ всегда существуют два локализованных у контакта решения уравнения (1):

$$\Psi_\pm = A \begin{pmatrix} \pm \exp(-i\theta/2) \\ 0 \\ 0 \\ \exp(i\theta/2) \end{pmatrix} \exp\left\{ -\frac{1}{2\hbar v_\parallel} \int_0^z \epsilon_g(z)dz + i\mathbf{k}_\perp \mathbf{r} \right\}, \qquad (2)$$

где $\mathbf{k}_\perp = (k_x, k_y, 0)$, $\exp(i\theta) = (k_x + ik_y)/k_\perp$. Подстановкой (2) в (1) можно убедиться, что в плоскости (x, y) функции $\Psi_\pm$ удовлетворяют уравнению Дирака с нулевой массой, унитарно эквивалентному уравнению Вейля. Соответствующий невырожденный безмассовый спектр

$$\epsilon_0^\pm(\mathbf{k}_\perp) = \pm \hbar v_\perp k_\perp \qquad (3)$$

Гамильтониан поверхностных электронных состояний

- $H = v_0(-i\underline{\partial} - e\underline{A})\underline{\sigma} + g_{eff}\underline{\sigma B}$

двумерный градиент вдоль поверхности

зеемановский член

Щель в спектре пропорциональна $g_{eff}B_z$

Сравним с графеном:

- один «дираковский» фермион вместо 4-х в графене (там 2 долины и 2 проекции спина)
- Псевдоспин из ур-ния Дирака – это «почти» реальный спин электрона (в графене – это индекс подрешеток, не связанный со спином)
- Поэтому магнитное поле $\perp$

Спектр поверхностных состояний ТИ в попереч

Quantum Spin Hall Insulator State in HgTe Quantum Wells

Markus König,[1] Steffen Wiedmann,[1] Christoph Brüne,[1] Andreas Roth,[1] Hartmut Buhmann,[1] Laurens W. Molenkamp,[1*] Xiao-Liang Qi,[2] Shou-Cheng Zhang[2]

Новая история: *Science* **318** 766 (2007)

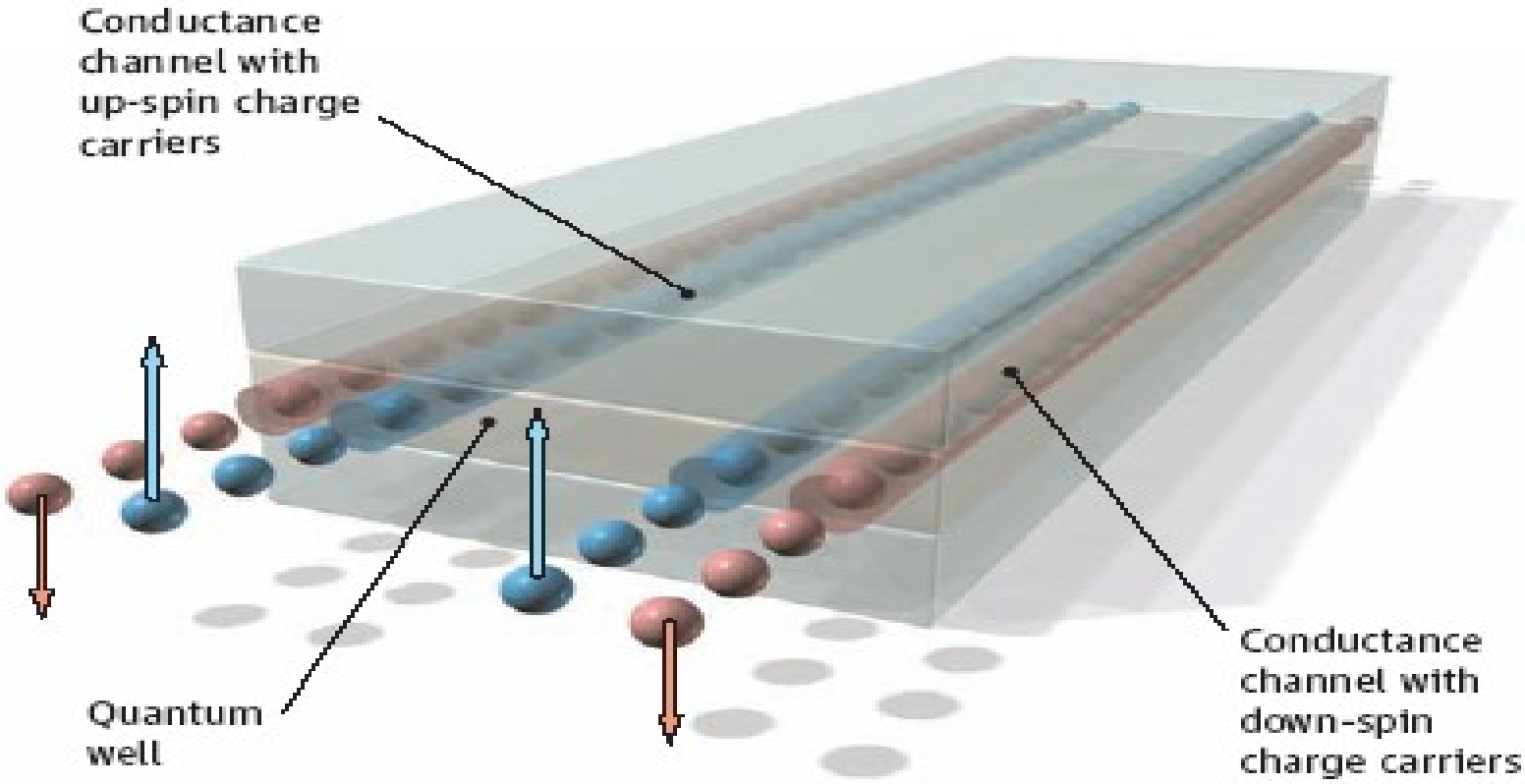

Schematic of the spin-polarized edge channels in a quantum spin Hall insulator.

$$H_{\text{eff}}(k_x,k_y) = \begin{pmatrix} H(k) & 0 \\ 0 & H^*(-k) \end{pmatrix},$$

$$H = \varepsilon(k) + d_i(k)\sigma_i$$

$$d_1 + id_2 = A(k_x + ik_y) \equiv Ak_+$$

$$d_3 = M - B(k_x^2 + k_y^2),$$

$$\varepsilon_k = C - D(k_x^2 + k_y^2).$$

M < 0 leads to surface anomaly

Recent theory predicted that the quantum spin Hall effect, a fundamentally new quantum state of matter that exists at zero external magnetic field, may be realized in HgTe/(Hg,Cd)Te quantum wells. We fabricated such sample structures with low density and high mobility in which we could tune, through an external gate voltage, the carrier conduction from n-type to p-type, passing through an insulating regime. For thin quantum wells with well width $d < 6.3$ nanometers, the insulating regime showed the conventional behavior of vanishingly small conductance at low temperature. However, for thicker quantum wells ($d > 6.3$ nanometers), the nominally insulating regime showed a plateau of residual conductance close to $2e^2/h$, where e is the electron charge and h is Planck's constant. The residual conductance was independent of the sample width, indicating that it is caused by edge states. Furthermore, the residual conductance was destroyed by a small external magnetic field. The quantum phase transition at the critical thickness, $d = 6.3$ nanometers, was also independently determined from the magnetic field–induced insulator-to-metal transition. These observations provide experimental evidence of the quantum spin Hall effect.

Краевые состояния не имеют рассеяния назад

No back-scattering !

- Спин однозначно связан с импульсом:

<1|2> = 0 *если нет явно спин-зависящего взаимодействия*

Что такое топологич. изолятор-2

Электродинамика с Θ-членом:

$$\Delta L_{axion} = \theta(e^2/2\pi hc)\mathbf{B}\cdot\mathbf{E}$$

Θ = π (2n+1) для сохранения Т-инвариантности

$$S_{3D} = \frac{2n+1}{8\pi}\int d^3x dt \epsilon^{\mu\nu\sigma\tau}\partial_\mu A_\nu \partial_\sigma A_\tau.$$

$\exp(iS_{3D}) = (-1)^n$

для интеграла по замкнутому пространству

зложение по материалу M. Franz, Physics **1**, 3

Что будет при $\Theta \neq$ const ?

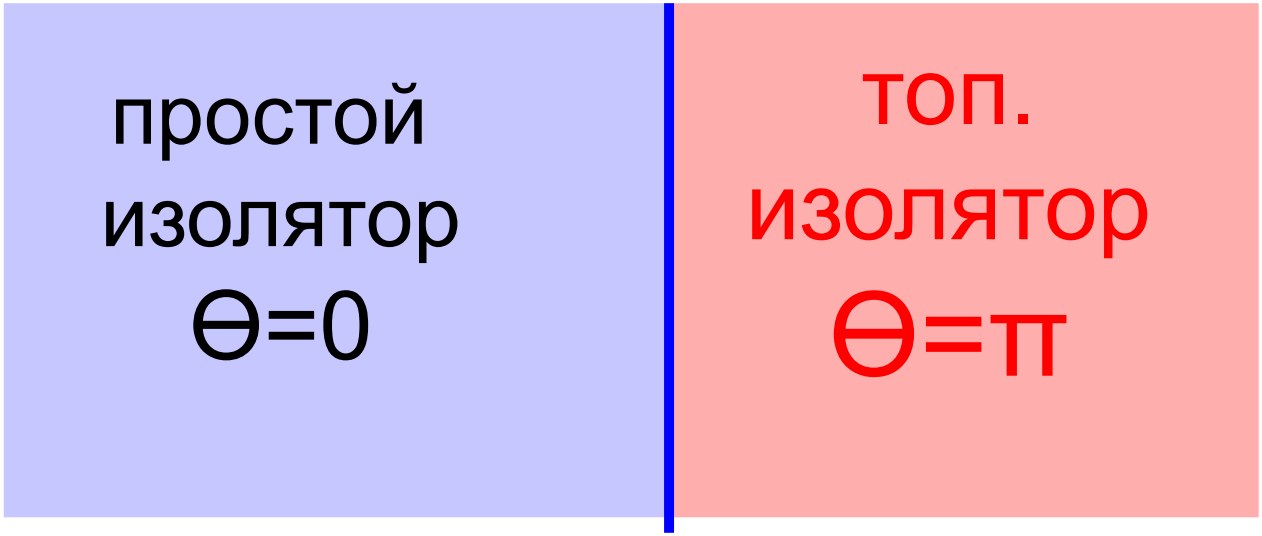

$$\nabla \cdot \mathbf{E} = \rho - (e^2/2\pi\hbar c)\nabla\theta \cdot \mathbf{B}$$

$$\nabla \times \mathbf{B} = \partial_t \mathbf{E} + \mathbf{j} + (e^2/2\pi hc)(\nabla\theta \times \mathbf{E} + \partial_t\theta \mathbf{B})$$

Аномальные члены сидят на границе

Магнито-электрический эффект

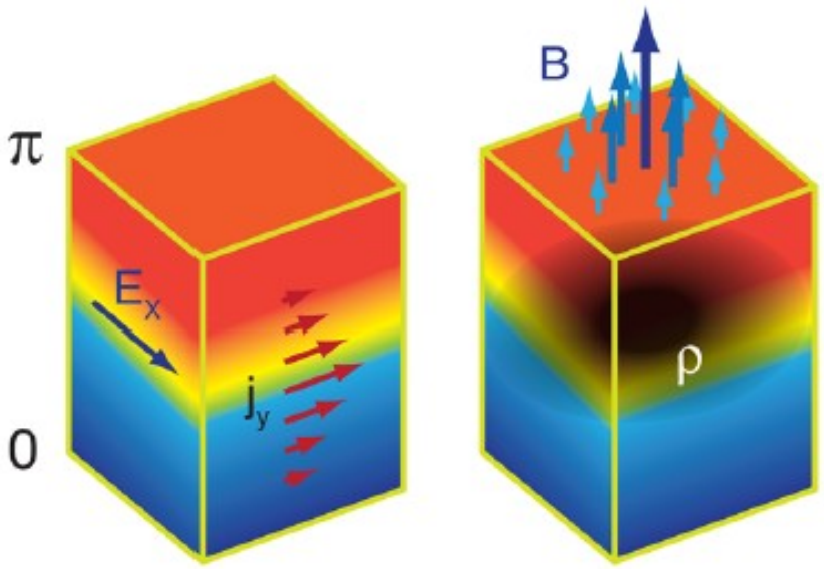

A magnetic field applied perpendicular to the same interface introduces $(n + 1/2)$ electrons for each flux quantum of applied field. The shaded region corresponds to the charge density, ρ, of the electrons, which mainly concentrates around the boundary between the two insulators and is largest where the magnetic field is strongest. (Illustration: Alan Stonebraker/`stonebrakerdesignworks.com`)

(Left) A quantum Hall effect occurs without strong magnetic field when an electric field applied in the plane of the interface between a topological (red region) and an ordinary (blue region) insulator (or vacuum) induces a precisely quantized current perpendicular to the field. (Right)

$$\sigma_H = (e^2/h)(n + 1/2)$$

Кроме того, эффект Керра – вращение плоскости поляризации отраженного света

известные как Топологические Изоляторы или Топ. Сверхпроводники

- 2D: HgTe (квантовые ямы с 2D электронами)
- 3D: $Bi_{1-x}Sb_x$ Bi_2Se_3 Bi_2Te_3 $Tl\,Bi\,Se_2$
- ^{3}He-B Н.Копнин et al J.LowTemp.Phys. 85, 267 (1991)

  Г.Волович Письма ЖЭТФ 90, 440 (2009).

  Topological superfluid ^{3}He-B: fermion zero modes on interfaces and in the vortex core M.A. Silaev, G.E. Volovik arXiv:1005.4672

Эксперименты ARPES

nature Vol 452|24 April 2008|doi:10.1038/nature06843

LETTERS

A topological Dirac insulator in a quantum spin Hall phase

D. Hsieh[1], D. Qian[1], L. Wray[1], Y. Xia[1], Y. S. Hor[2], R. J. Cava[2] & M. Z. Hasan[1,3]

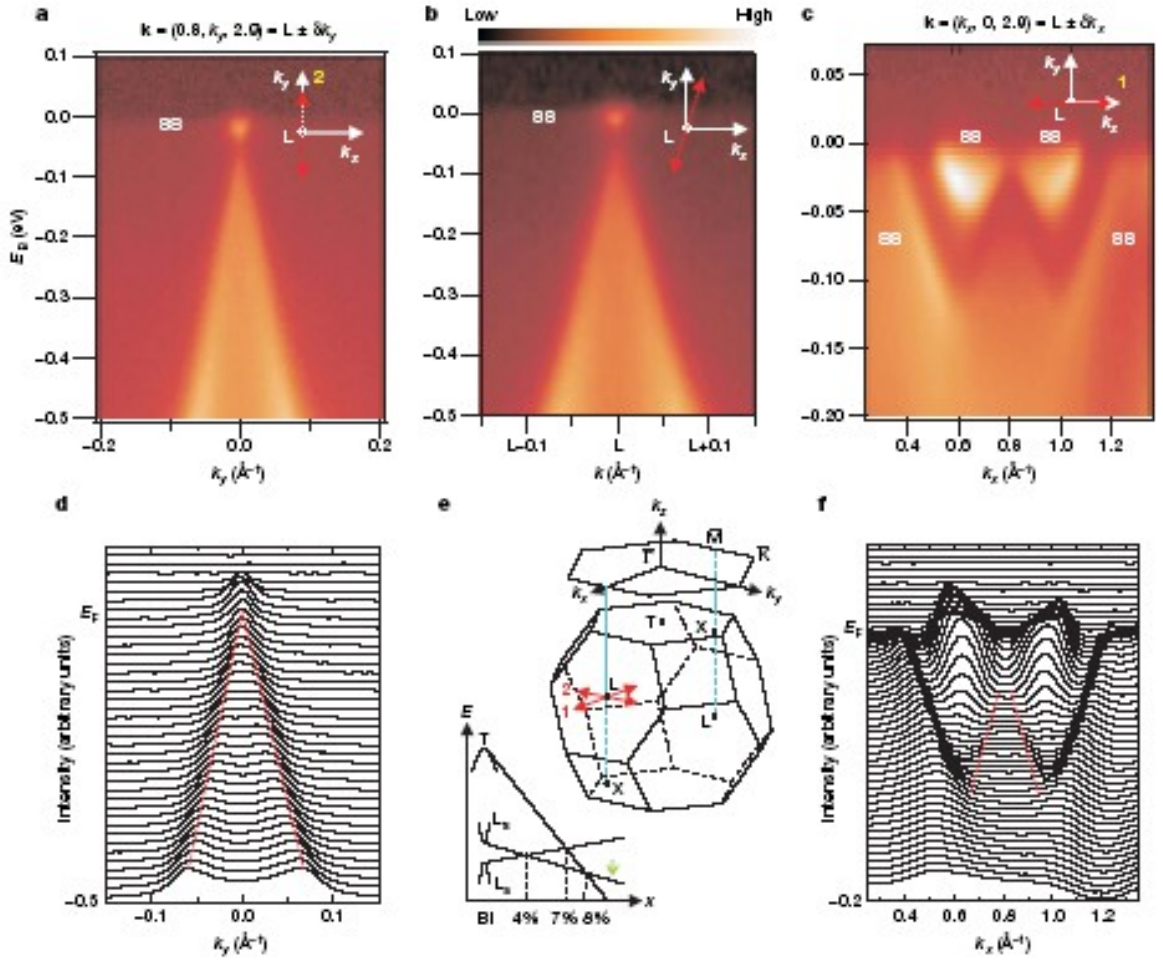

Figure 1 | Dirac-like dispersion near the L-point in the bulk Brillouin zone. Selected ARPES intensity maps of $Bi_{0.9}Sb_{0.1}$ are shown along three **k**-space cuts through the L-point of the bulk 3D Brillouin zone. The presented data are taken in the third Brillouin zone with $L_z = 2.9\,\text{Å}^{-1}$ with a photon energy of 29 eV. The cuts are along the k_y-direction (**a**); a direction rotated by approximately 10° from the k_y-direction (**b**); and the k_x-direction (**c**). Here, δ symbolizes a change along a particular **k**-direction. Each cut shows a Λ-shaped bulk band whose tip lies below the Fermi level, signalling a bulk gap. The surface states are denoted SS and are all identified in Fig. 2 (for further identification via theoretical calculations, see Supplementary Information). **d**, Momentum distribution curves corresponding to the intensity map in **a**. **f**, A log-scale plot of the momentum distribution curves corresponding to the intensity map in **c**. The red lines are guides to the eye for the bulk features in the momentum distribution curves. **e**, Schematic of the bulk 3D Brillouin zone of $Bi_{1-x}Sb_x$ and the 2D Brillouin zone of the projected (111) surface. The high-symmetry points $\bar{\Gamma}$, $\bar{M}$ and $\bar{K}$ of the surface Brillouin zone are labelled. The schematic evolution of bulk band energies as a function of x is shown. The L-band inversion transition occurs at $x \approx 0.04$, where a 3D gapless Dirac point is realized, and the composition we study here (for which $x = 0.1$) is indicated by the green arrow. A more detailed phase diagram based on our experiments is shown in Fig. 3c.

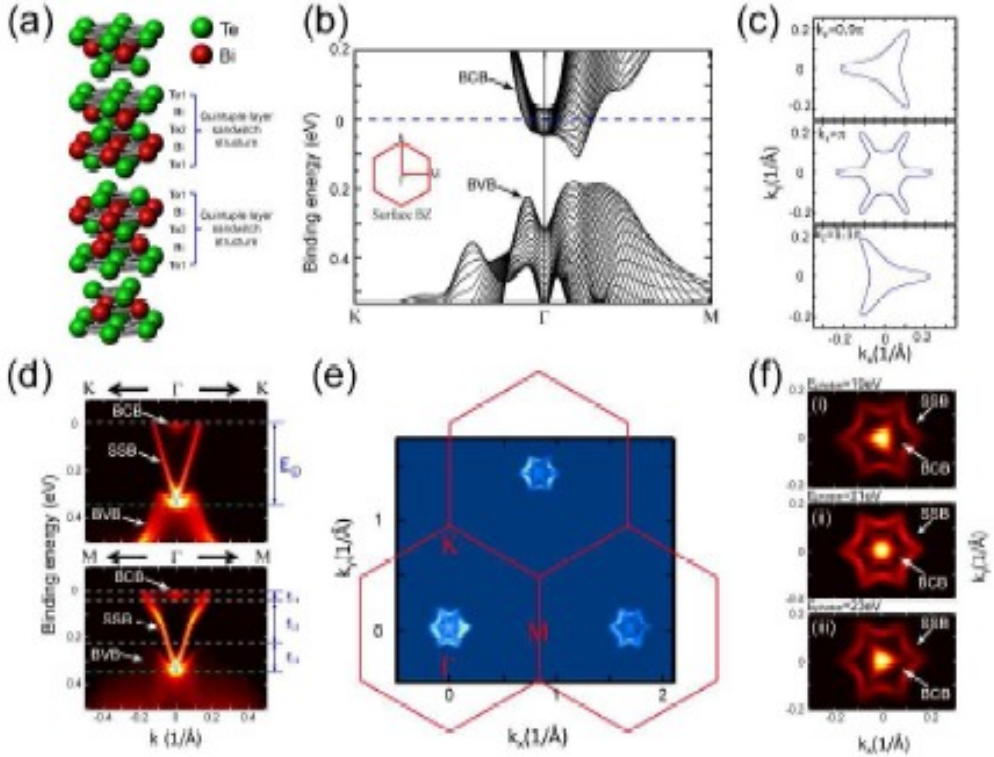

FIG. 1: (Color) Crystal and electronic structures of Bi_2Te_3 (a) Tetradymite-type crystal structure of Bi_2Te_3, formed by stacking quintuple-layer groups sandwiched by three sheets of Te and two sheets of Bi. (b) Calculated bulk conduction band(BCB) and bulk valance band(BVB) dispersions along high symmetry directions of the surface BZ (see inset), with the chemical potential rigidly shifted to 45meV above the BCB bottom at to match the experimental result. (c) The k_z dependence of the calculated bulk FS projection on the surface BZ. (d) ARPES measurements of band dispersions along $K-\Gamma-K$(top) and $M-\Gamma-M$ (bottom) directions. The broad bulk band (BCB and BVB) dispersions are similar to those in panel (b), while the sharp V-shape dispersion is from the surface state band (SSB). Energy scales of the band structure are labeled as: E_0: Binding energy of Dirac point (0.34eV), E_1: BCB bottom binding energy(0.045eV), E_2:bulk energy gap(0.165eV) and E_3: energy separation between BVB top and Dirac point (0.13eV). (e) Measured wide range FS map covering three BZs shows that the FSs only exist around Γ point, where the red hexagons represent the surface BZ. The uneven intensity of the FSs at different BZs results from the matrix element effect. (f) Photon energy dependent FS maps. The shape of the inner FS changes dramatically with photon energies, indicating a strong k_z dependence due to its bulk nature as predicted in panel (c), while the non-varying shape of the outer hexagram FS confirms its surface state origin.

Topological Insulators with Inversion Symmetry

Liang Fu and C.L. Kane

Phys Rev B
76, 045302 (2007)
75, 195312 (2006)

Bloch wavefunctions

$$|\psi_{n,\mathbf{k}}\rangle = e^{i\mathbf{k}\cdot\mathbf{r}}|u_{n,\mathbf{k}}\rangle.$$

We require $|\psi_{n,\mathbf{k}+\mathbf{G}}\rangle = |\psi_{n,\mathbf{k}}\rangle$ for reciprocal lattice vectors $\mathbf{G}$, so that the Brillouin zone in which $\mathbf{k}$ is defined is a torus. This implies $|u_{n,\mathbf{k}+\mathbf{G}}\rangle = e^{-i\mathbf{G}\cdot\mathbf{r}}|u_{n,\mathbf{k}}\rangle$. Time reversal symmetry implies $[\mathcal{H}, \Theta] = 0$, where $\Theta = \exp(i\pi S_y)K$

$\Theta^2 = -1$. It follows that $H(-\mathbf{k}) = \Theta H(\mathbf{k})\Theta^{-1}$.

There are special points $\mathbf{k} = \Gamma_i$ in the Brillouin zone which are time reversal invariant and satisfy $-\Gamma_i = \Gamma_i + \mathbf{G}$ for a reciprocal lattice vector $\mathbf{G}$. There are eight such points in three dimensions and four in two dimen-

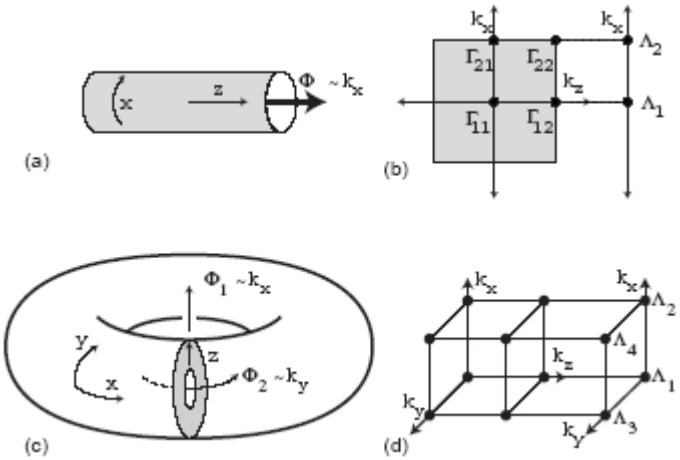

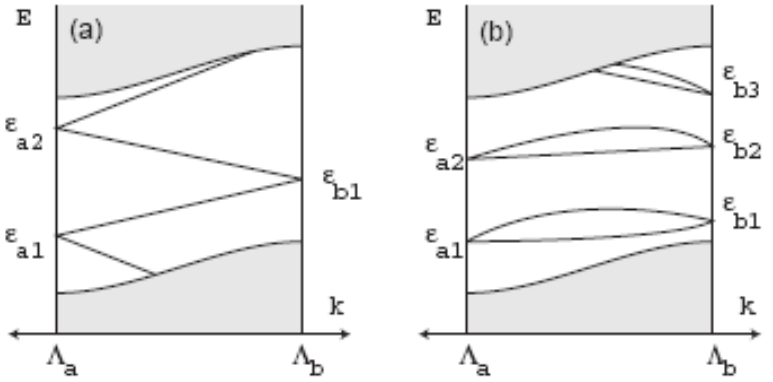

FIG. 2: Schematic representations of the surface energy levels of a crystal in either two or three dimensions as a function of surface crystal momentum on a path connecting Λ_a and Λ_b. The shaded region shows the bulk continuum states, and the lines show discrete surface (or edge) bands localized near one of the surfaces. The Kramers degenerate surface states at Λ_a and Λ_b can be connected to each other in two possible ways, shown in (a) and (b), which reflect the change in time reversal polarization $\pi_a\pi_b$ of the cylinder between those points. Case (a) occurs in topological insulators, and guarantees the surface bands cross any Fermi energy inside the bulk gap.

$$\delta_i = \frac{\sqrt{\det[w(\Gamma_i)]}}{\mathrm{Pf}[w(\Gamma_i)]} = \pm 1,$$

$2N \times 2N$ unitary matrix

$$w_{mn}(\mathbf{k}) \equiv \langle u_{m-\mathbf{k}}|\Theta|u_{n\mathbf{k}}\rangle.$$

$$\langle \Theta a|\Theta b\rangle = \langle b|a\rangle \text{ and } \Theta^2 = -1$$

$$(-1)^{\nu} = \prod_{i=1}^{4} \delta_i.$$

$$(-1)^{\nu_0} = \prod_{i=1}^{8} \delta_i \qquad (-1)^{\nu_k} = \prod_{n_k=1; n_{j\neq k}=0,1} \delta_{i=(n_1 n_2 n_3)}.$$

Topological field theory of time-reversal invariant insulators
Xiao-Liang Qi, Taylor L. Hughes and Shou-Cheng Zhang
Phys. Rev. B **78**, 195424 (2008) – Published November 24, 2008

TRB TOPOLOGICAL INSULATORS IN 2 + 1 DIMENSIONS AND ITS DIMENSIONAL REDUCTION

$$H = \sum_{\mathbf{k}} c^{\dagger}_{\mathbf{k}\alpha} h^{\alpha\beta}(\mathbf{k}) c_{\mathbf{k}\beta} \qquad H \simeq \sum_{\mathbf{k}} c^{\dagger}_{\mathbf{k}} h(\mathbf{k}) c_{\mathbf{k}} + \sum_{\mathbf{k},\mathbf{q}} A^{i}(-\mathbf{q}) c^{\dagger}_{\mathbf{k}+\mathbf{q}/2} \frac{\partial h(\mathbf{k})}{\partial k_i} c_{\mathbf{k}-\mathbf{q}/2}$$

$$\sigma_{xy} = \frac{e^2}{h}\frac{1}{2\pi}\int dk_x \int dk_y f_{xy}(\mathbf{k}) \qquad C_1 = \frac{1}{2\pi}\int dk_x \int dk_y f_{xy}(\mathbf{k}) \in \mathbb{Z}$$

$$\text{with } f_{xy}(\mathbf{k}) = \frac{\partial a_y(\mathbf{k})}{\partial k_x} - \frac{\partial a_x(\mathbf{k})}{\partial k_y}$$

$$a_i(\mathbf{k}) = -i \sum_{\alpha \in \text{ occ}} \langle \alpha \mathbf{k} | \frac{\partial}{\partial k_i} | \alpha \mathbf{k} \rangle, \ i = x, y. \qquad j_i = \sigma_H \epsilon^{ij} E_j$$

$$\rho(B) - \rho_0 = \sigma_H B$$

$$j^{\mu} = \frac{C_1}{2\pi}\epsilon^{\mu\nu\tau}\partial_{\nu} A_{\tau} \qquad S_{\text{eff}} = \frac{C_1}{4\pi}\int d^2x \int dt A_{\mu}\epsilon^{\mu\nu\tau}\partial_{\nu} A_{\tau},$$

$$e = \hbar = 1$$

Example: two band models

$$h(\mathbf{k}) = \sum_{a=1}^{3} d_a(\mathbf{k})\sigma^a + \epsilon(\mathbf{k})\mathbb{I}$$

The occupied band satisfies

$(\mathbf{d}(\mathbf{k})\cdot\sigma)\,|-,\mathbf{k}\rangle = -\,|\mathbf{d}(\mathbf{k})|\,|-,\mathbf{k}\rangle$, which thus corresponds to the spinor with spin polarization in the $-\mathbf{d}(\mathbf{k})$ direc-

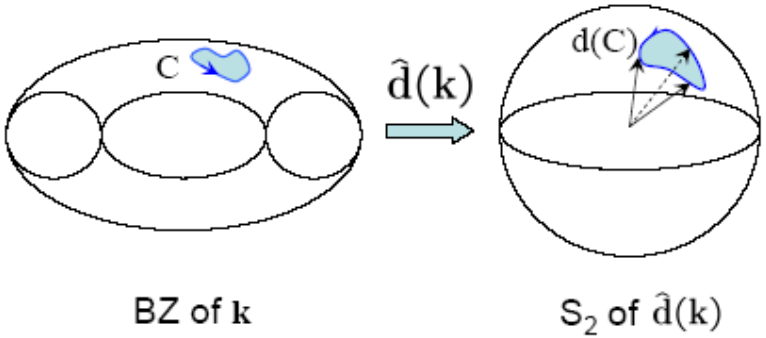

$$C_1 = \frac{1}{4\pi}\int dk_x \int dk_y \hat{\mathbf{d}}\cdot\frac{\partial\hat{\mathbf{d}}}{\partial k_x}\times\frac{\partial\hat{\mathbf{d}}}{\partial k_y}.$$

$$\begin{aligned} h(\mathbf{k}) &= (\sin k_x)\sigma_x + (\sin k_y)\sigma_y \\ &\quad + (m + \cos k_x + \cos k_y)\,\sigma_z, \end{aligned}$$

FIG. 1: Illustration of the Berry's phase curvature in a two-band model. The Berry's phase $\oint_C \mathbf{A}\cdot\mathbf{dr}$ around a path C in the BZ is half of the solid angle subtended by the image path $d(C)$ on the sphere S_2.

$$C_1 = \begin{cases} 1, & 0 < m < 2 \\ -1, & -2 < m < 0 \\ 0, & \text{otherwise.} \end{cases}$$

Непрерывный предел: 0< m +2 << 1

$$h(\mathbf{k}) = \begin{pmatrix} m+2 & k_x - ik_y \\ k_x + ik_y & -m-2 \end{pmatrix}$$

Crossover of Three-Dimensional Topological Insulator of Bi_2Se_3 to the Two-Dimensional Limit

Yi Zhang[1], Ke He[1*], Cui-Zu Chang[1,2], Can-Li Song[1,2], Li-Li Wang[1], Xi Chen[2], Jin-Feng Jia[2], Zhong Fang[1], Xi Dai[1], Wen-Yu Shan[3], Shun-Qing Shen[3], Qian Niu[4], Xiao-Liang Qi[5], Shou-Cheng Zhang[5], Xu-Cun Ma[1], and Qi-Kun Xue[1,2*]

Nature Phys. **6**, 584 (2010)

QL	E_0 (eV)	D (eV·Å^2)	Δ (eV)
2	-0.470	-14.4	0.252
3	-0.407	-9.7	0.138
4	-0.363	-8.0	0.070
5	-0.345	-15.3	0.041
6	-0.324	-13.0	0

$$E_{\pm}(k_{//}) = E_0 - Dk_{//}^2 \pm \sqrt{(v_F \hbar k_{//})^2 + (\frac{\Delta}{2} - Bk_{//}^2)^2}$$

$$E_{\sigma\pm}(k_{//}) = E_0 - Dk_{//}^2 \pm \sqrt{(|\vec{V}'| + \sigma v_F \hbar k_{//})^2 + (\frac{\Delta}{2} - Bk_{//}^2)^2}$$

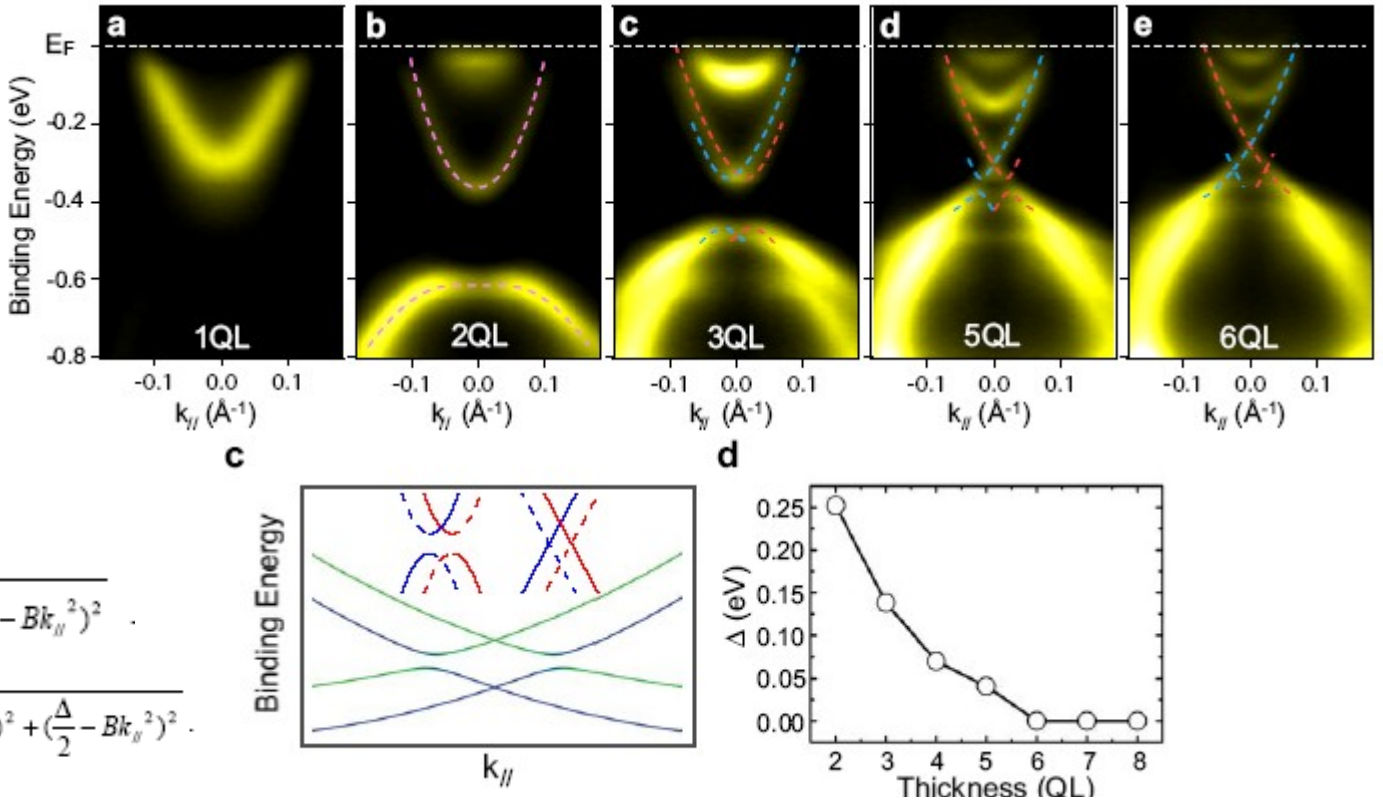

Green and blue colours represent the states that mainly localize at surface and interface, respectively. The inset shows a schematic illustration of the surface states of Bi_2Se_3 film above (right) and below (left) 6 QL. The solid and dashed lines represent the surface states that mainly localize at surface and interface of Bi_2Se_3 film, respectively. The red and blue colours of the lines represent different spins. **d**,

а ч а 5 Найти щель
ектре поверхностных
тоянний из-за перекрытия
новых функций верхней
жней поверхностей

Туннель для связи с антиподами

Yi Zhang, Ying Ran, Ashvin Vishwanath

arxiv:0904.0690

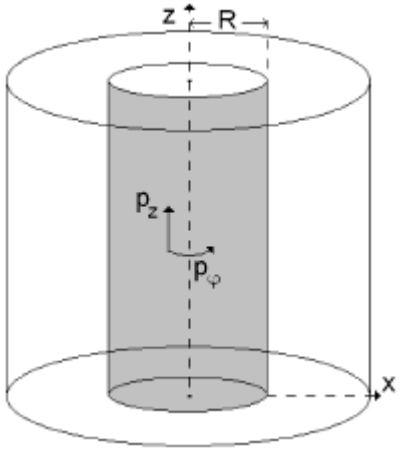

Тонкая бесконечная пластинка ТИ

На верхней и нижней поверхностях живут дираковские электроны

Сквозной туннель радиуса R содержит на внутренней поверхности

$$E_n^2(k) = \hbar^2(k^2 + n^2/R^2)$$

n = m + ½ - (Φ/Φ_0)

m – целое число

$\Phi_0 = hc/e$ - квант магнитного потока

Вывести эту формулу для спектра состояний в т

Signatures of Majorana fermions in hybrid superconductor-semiconductor nanowire devices

V. Mourik, K. Zuo, S.M. Frolov, S.R. Plissard, E.P.A.M. Bakkers, L.P. Kouwenhoven

Figure S1: N-NW-S device fabrication

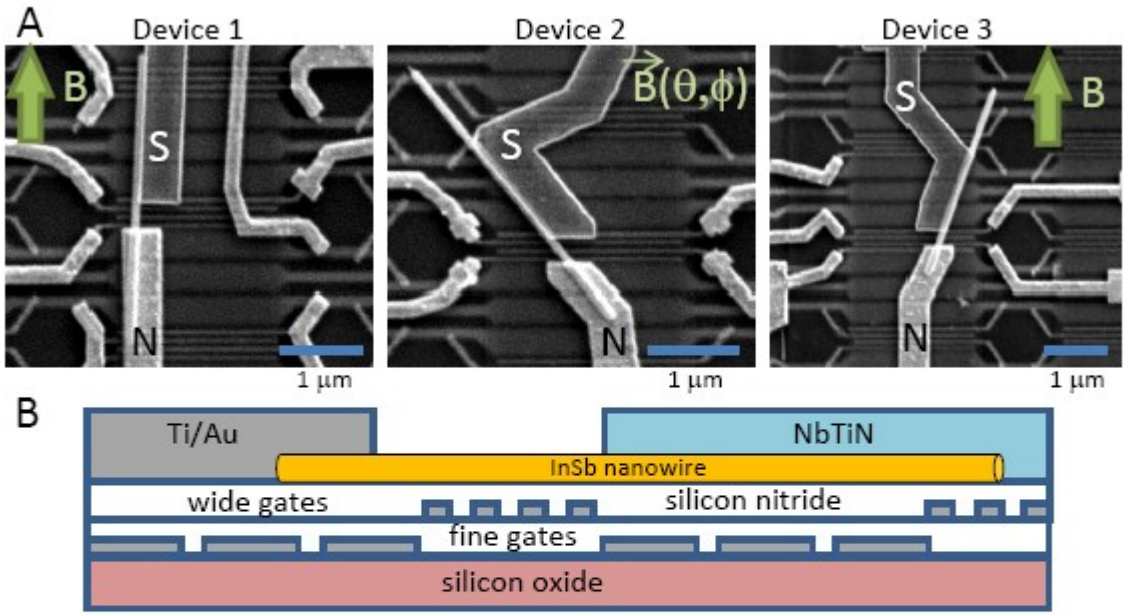

A, SEM images of three N-NW-S (Normal-Nanowire-Superconductor) devices in which the main findings of this paper are reproduced. Field directions are indicated with arrows. Device 2 was measured in a 3-axis vector magnet. Devices are fabricated simultaneously. Nanowire diameters are 110±10 nm (devices 1 and 3) and 100±10 nm (device 2). **B**, Schematic of a device cross-section.

Nanowire growth details. InSb nanowires are grown by metalorganic vapor phase epitaxy from gold catalysts, as described in Ref. (*15*). The wires in this work are grown on Si substrates. First, stems that consists of InP and InAs segments are grown. Then a stacking-fault and dislocation-free zincblende InSb segment of high mobility (10^4-$5{\cdot}10^4$cm^2/(Vs) is grown in the 111 crystal direction. A single batch of wires is used for all N-NW-S devices in this paper.